IOP Conf. Series: Materials Science and Engineering **256** (2017) 012004 doi:10.1088/1757-899X/256/1/012004

Multi-frequency data analysis in AFM by wavelet transform

V Pukhova[1,*] and G Ferrini[2]

[1]Department of Quantum Electronics and Optoelectronic Devices, Saint Petersburg Electrotechnical University "LETI", Saint Petersburg, 197376, Russia
[2]Interdisciplinary Laboratories for Advanced Materials Physics (I-LAMP) and Dipartimento di Matematica e Fisica, Università Cattolica del Sacro Cuore, Brescia, 25121, Italy

[*]vmpukhova@etu.ru

Abstract. Interacting cantilevers in AFM experiments generate non-stationary, multi-frequency signals consisting of numerous excited flexural and torsional modes and their harmonics. The analysis of such signals is challenging, requiring special methodological approaches and a powerful mathematical apparatus. The most common approach to the signal analysis is to apply Fourier transform analysis. However, FT gives accurate spectra for stationary signals, and for signals changing their spectral content over time, FT provides only an averaged spectrum. Hence, for non-stationary and rapidly varying signals, such as those from interacting cantilevers, a method that shows the spectral evolution in time is needed. One of the most powerful techniques, allowing detailed time-frequency representation of signals, is the wavelet transform. It is a method of analysis that allows representation of energy associated to the signal at a particular frequency and time, providing correlation between the spectral and temporal features of the signal, unlike FT. This is particularly important in AFM experiments because signals nonlinearities contains valuable information about tip-sample interactions and consequently surfaces properties. The present work is aimed to show the advantages of wavelet transform in comparison with FT using as an example the force curve analysis in dynamic force spectroscopy.

1. Introduction

Scanning probes used in Atomic Force Microscopy (AFM) [1] are micromechanical oscillators and the theory of AFM dynamics is based on the analysis of the oscillating frequencies of beam resonators. Interacting cantilevers in AFM experiments generate non-stationary, multi-frequency signals consisting of numerous excited flexural and torsional modes and their harmonics.

In conventional dynamic AFM methods the excitation and detection of the cantilever oscillations are performed at a single frequency. While the tip is interacting with the surface, higher frequency components in the cantilever dynamics arise caused by the nonlinearities in the interaction force. These components carry information about the sample properties. The existence of these additional components in the detected signal has been known for several years, but their role in the cantilever dynamic, spatial resolution, and sensitivity to material properties was not appreciated.

The oscillations of a non-interacting cantilever driven at frequency ω are nearly perfect sinusoids that can be described as $Acos(\omega t + \varphi)$, where A is the amplitude of the oscillations and φ is the phase lag with respect to the driver. When the tip of the excited cantilever comes in close vicinity of the sample surface, it starts experiencing distortions because of forces acting on the tip and this leads to

the excitation of higher harmonics [2, 3]. Thus, the frequency spectrum of the higher harmonics contains detailed information on the nonlinearities of the tip-sample interaction forces [4, 5]. The contribution of the components containing higher harmonics in the cantilever motion can be described as $\sum_{n=1}^{\infty} a_n \cos(n\omega t + \varphi_n)$, where a_n is the amplitude (note that it decreases as $1/n^2$) and φ_n is the phase shift of the n-harmonic, n is an integer number. In general, the higher harmonics provide enhanced lateral resolution, because the frequency shift due to the tip-sample interaction is amplified by a factor of n for the n-th harmonic [6, 7]. The higher harmonics amplitudes are not influenced by the surface topography, but by the borders of patterns, where the geometry of the tip-sample contact varies. Because of this, the excited higher harmonics provide high sensitivity to the surface roughness [6]. In the case of heterogeneous samples, the amplitudes of the higher harmonics change with respect to the mechanical properties of the regions. They can also be used to probe the elastic properties and dissipative forces [8, 9] and to perform the compositional mapping in air [10] and liquid environments [11, 12].

The higher harmonics should be distinguished from the higher modes of the cantilever. The higher harmonics are consecutive integer multiples of the fundamental cantilever resonance. The higher eigenfrequencies of the oscillating beam, however, do not form a series of consecutive integer multiples [13]. As an example, for rectangular cantilever the frequency of the second eigenmode ($6.27f$) is close to the sixth harmonic ($6f$). The values of the frequencies of the higher harmonics are close to those of the flexural eigenmodes of the cantilever. This leads to the fact that the higher harmonics act as driving forces and are able to excite the higher modes of the cantilever that are close to the integer multiples of the fundamental mode. This nonlinear modal interaction is called internal resonance [2, 6]. So, when the tip is close to the surface and is influenced by the nonlinear surface interaction forces, higher harmonics are excited. And these higher harmonics excite the oscillations of the higher eigenmodes of the cantilever due to the internal resonance. The higher modes contribute to the motion of the cantilever as $\sum_{i=1}^{\infty} b_i \cos(\omega_i t + \psi_i)$, where ω_i is the frequency, b_i is the amplitude and ψ_i is the phase shift of the i-eigenmode, i is an integer number [14]. The variations in the oscillating parameters of the higher eigenmodes are very sensitive to changes in the tip-sample interaction forces, consequently increasing the sensitivity to the mechanical, magnetic, or electric tip-sample interactions [15-17].

A number of techniques have been implemented to gain information from the tip-sample interactions, but usually the interaction of the tip with the surface is revealed by the modification of the average value of the amplitude, frequency, and phase shift over many oscillation cycles [18, 19]. The averaging techniques provide superior sensibility, allowing to probe the details of force interactions down to the molecular level [18], but they are not allowing to capture the information conveyed by the sensing tip in a single interaction, during few oscillation cycles of the cantilever. This article concentrates on the analysis technique that is able to characterize all cantilever frequency components at once, without averaging.

2. Data analysis technique

The goal of any AFM experiment is to gain information about the properties of the sample surface encoded in the dynamics of the cantilever by exploring the characteristics of the signal via signal transformation.

The most common approach to the signal analysis is to apply the Fourier transform (FT) analysis, which decomposes the signal into constituent frequencies displayed in the spectrum as resonance peaks [20]. Attributing these peaks to the frequencies that caused them in the case of stationary signals is an easy task, but it can be challenging for non-stationary signals since their spectral characteristics change over time. FT analysis gives meaningful spectra in case of stationary signals. For non-stationary and rapidly varying signals, which spectral content changes over time, such as those from interacting cantilevers in AFM experiments, FT provides an averaged spectrum, which is integrated over the whole acquisition time. Hence, to analyze this type of signals, a method that allows representing the spectral evolution in time is needed.

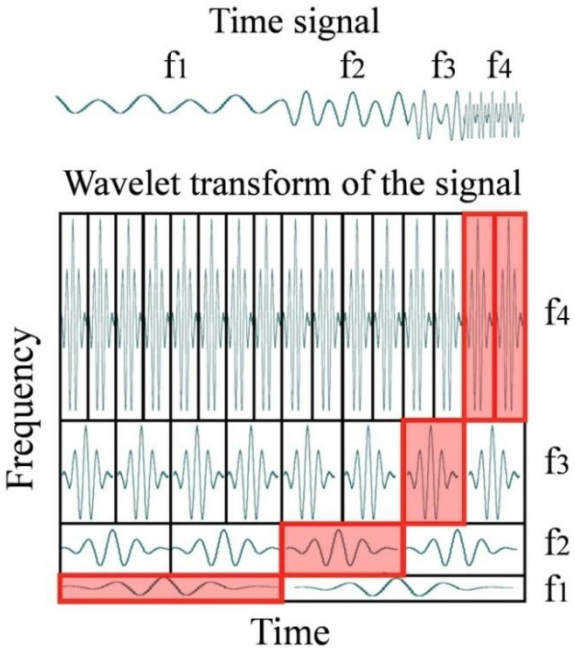

Figure 1. Principle of the WT technique.

One of the techniques allowing detailed time-frequency representation of the signals is the wavelet transform (WT) [20, 21]. WT is a method of analysis that allows representation of energy associated to the signal at a particular frequency and time, providing correlation between the spectral and temporal features of the signal. This is particularly important in AFM, because signals nonlinearities contain valuable information about tip-sample interactions and, consequently, surfaces properties [22-25].

The wavelet is an oscillating waveform function with limited support in time and zero average. The WT of the signal is the projection of the time signal onto a set of scaled and delayed wavelets; hence, the WT gives a two-dimensional time-frequency representation of a temporal signal. The original wavelet is called a mother wavelet and scaled and delayed wavelets are called daughter wavelets. The mother wavelet should be chosen according to the characteristics of the signal and the data analysis task [20].

The daughter wavelets are determined as [20]:

$$\Psi_{s,d}(t) = \frac{1}{\sqrt{s}}\Psi\left(\frac{t-d}{s}\right), \tag{1}$$

where $\Psi(t)$ is the mother wavelet, s is the positive adimensional scale parameter (stretches or compresses the mother wavelet and is connected to the frequency) and d is the delay parameter (shifts the wavelet along the time axis and is connected to the time).

The WT of the signal is determined as [20]:

$$W^f(s,d) = \int_{-\infty}^{+\infty} f(t)\Psi_{s,d}^*(t)dt = \int_{-\infty}^{+\infty} f(t)\frac{1}{\sqrt{s}}\Psi^*\left(\frac{t-d}{s}\right)dt, \tag{2}$$

where $f(t)$ is a temporal signal and $W^f(s,d)$ are wavelet coefficients that display a comparative similarity between the signal and the particular daughter wavelet function.

To illustrate the principle of the WT technique, consider the analysis of the time signal presented in Figure 1. The time signal is a sequence of several signals of different frequencies, which appear consecutively one after another. The first half of the signal is of frequency f_1, followed by the signal of frequency f_2 (quarter of the total signal duration), the next part of the signal is of frequency f_3 (eighth part of the total signal duration), and the remaining part of the signal is of frequency f_4, where $f_1 < f_2 < f_3 < f_4$. Wavelet analysis transforms the signal into a two-dimensional time-frequency representation. This two-dimensional space is orderly filled with the daughter wavelets, so that the

vertical axis shows the change of the frequency, which is connected to the scale parameter, and the horizontal axis shows the change of the time, which is connected to the delay parameter, as shown in Figure 1. The wavelet transform, in this case, is carried out in the following way: each daughter wavelet from the two-dimensional time-frequency plane is compared with the corresponding part of the analyzed signal. The magnitude of the similarity between the analyzed part of the signal and the particular daughter wavelet gives the value of the wavelet coefficient, which is encoded in the time-frequency domain according to a given rule. The regions corresponding to the highest similarity between the parts of the signal and the daughter wavelets from the time-frequency plane are highlighted (Fig. 1 – red areas). According to this principle, the result of the wavelet analysis is the wavelet spectrum, schematically shown in Figure 1. From the WT spectrum it is possible to extract not only the set of frequencies constituting the signal, but also the exact frequency forming the signal at each moment.

The full spectral response of the signal can be provided, if the phase analysis is performed simultaneously with the amplitude analysis. The phase analysis is based on the cross-wavelet transform (XWT) [23].

The XWT spectrum of two signals $h(t)$ and $g(t)$ is defined as [20]:

$$W^{hg}(s,d) = W^{h}(s,d)W^{g*}(s,d), \tag{3}$$

where $W^{hg}(s,d)$ are the cross-wavelet amplitudes, $W^{h}(s,d)$ and $W^{g*}(s,d)$ are the WT of the time signals and $*$ symbolizes the complex conjugate.

The comparative phase difference between the two time signals at particular time-frequency moment (s,d) is defined as [20]:

$$\Phi^{hg}(s,d) = \Phi^{h}(s,d) - \Phi^{g}(s,d) = tan^{-1}\left(\frac{\Im(<s^{-1}W^{hg}(s,d)>)}{\Re(<s^{-1}W^{hg}(s,d)>)}\right), \tag{4}$$

where $\Phi^{h}(s,d)$ is the phase of signal $h(t)$, $\Phi^{g}(s,d)$ is the phase of signal $g(t)$, $<>$ represents the smoothing operator, $\Re$ and $\Im$ are the real and imaginary parts, respectively.

Taking into account that the signal consists of a sum of Fourier components oscillating at different frequencies, the phases of each component of the time signal can be measured, if a reference signal at the same frequency is available. It is convenient to have a *sinc* ("sinus cardinalis") function as a reference signal [23]. The *sinc* function is composed of a superposition of a number of cosines that have a maximum at zero time and oscillation frequencies in the interval between zero and maximal cut-off frequency. Since the time width of the *sinc* function is inversely proportional to its bandwidth, it gives the phase reference only near zero time. To have a phase reference at other times, the *sinc* function has to be translated along the time scale to the points of interest. Measuring by the XWT the instantaneous phase difference between the signal and the time-translated reference, *sinc* function allows forming a "phase carpet" in the time-frequency plane [23].

To illustrate the principle of the XWT technique, consider the analysis of the signal shown in Figure 2. The signal (gray line) consists of a sum of two cosines oscillating at different frequencies, $f_1 = 12$ kHz (blue line) and $f_2 = 6.5f_1 = 75$ kHz (green line), with an amplitude ratio of $A_1{:}A_2 = 3{:}1$, where A_1 and A_2 are the amplitudes of cosines components of the signal, and zero phase at zero time for both components (Fig. 2a). In Figure 2b the wavelet analysis of the signal in Figure 2a is shown. In Figure 2b the wavelet coefficients are coded in a color-scale and it can be seen that two oscillating components that combine the signal are highlighted, so the red line corresponds to the component with frequency f_1 and the green line to the one with frequency f_2. The relative phase obtained as a result of the wavelet cross-correlations between the analyzed signal and the reference *sinc* function is coded in the slope of the arrows superposed on the wavelet spectra. Black arrows correspond to the component with frequency f_1, red arrows – to the one with frequency f_2, and gray arrows show edge effect; the other frequencies are absent in the signal. Arrows pointing right indicate 0°, left – 180°, up – -90° and down – 90° of relative phase shift between the time signal and reference *sinc* function. The intermediate phases are in between these values.

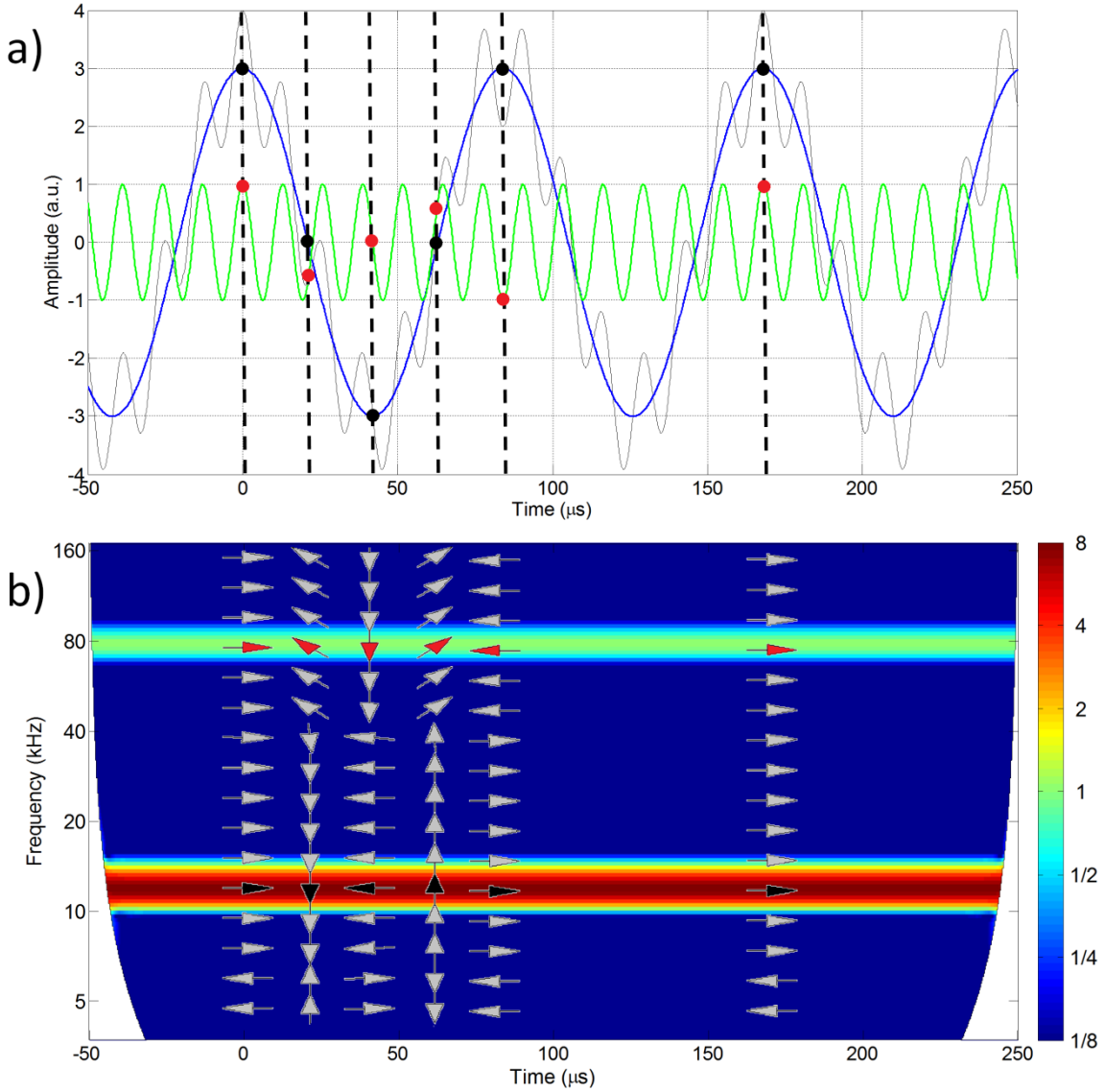

Figure 2. Principle of the XWT technique. (a) The signal (gray line) consists of a sum of two cosines oscillating at frequencies $f_1 = 12$ kHz (blue line) and $f_2 = 6.5f_1 = 75$kHz (green line), with an amplitude ratio of $A_1 : A_2 = 3 : 1$, and zero phases at time zero for both components. The black dashed lines correspond to time moments (from left to right): $0, \frac{T}{4}, \frac{T}{2}, \frac{3T}{4}, T$, and $2T$, where $T = 1/f_1$. (b) XWT analysis of the signal at time moments $0, \frac{T}{4}, \frac{T}{2}, \frac{3T}{4}, T$, and $2T$. The wavelet coefficients are coded in a color-scale. Both color-scale and frequency axes have base-2 logarithm scales. Edge artifacts of the WT are delimited by a white shade.

The black dashed lines in Figure 2a correspond to time moments (from left to right): $0, \frac{T}{4}, \frac{T}{2}, \frac{3T}{4}, T$, and $2T$, where $T = 1/f_1$, and the XWT analysis at these time moments is shown in Figure 2(b). At the zero time both oscillating components of the signal and *sinc* function are in phase; hence, the phase shifts are equal 0° (black and red arrows are pointing right). Moving the reference *sinc* function along time scale and measuring the relative phase shift between the oscillating components of the signal and *sinc* at time moments $\frac{T}{4}, \frac{T}{2}, \frac{3T}{4}, T$ we can verify that for the component with frequency f_1 the phase shifts are successively equal to 90°, 180°, -90°, and 0°, and for the component with frequency f_2 the

phase shifts are successively equal to -135°, 90°, -45°, and 180°. To have both oscillating components of the signal and *sinc* function in phase, as it is at zero time, we need to move to the shortest common multiple period, i.e. 2*T* (both red and black arrows are pointing right).

3. Multi-frequency representation of the signals by wavelet transform

The AFM allows not only to investigate the topography of surfaces, but also to study the properties of surfaces by measuring tip-sample forces, commonly known as force spectroscopy. The curves obtained during force spectroscopy experiments are called force curves [26, 27].

To exemplify the data analysis technique based on the WT, a force curve is investigated, in order to show the evolution of the signal spectrum during a dynamic force spectroscopy experiment. The force spectroscopy experiment requires sequential measurements of the magnitude of the cantilever deflection due to the action of forces on its tip, while it approaches the sample surface. These measurements are generally performed at a number of fixed distances from the sample surface. When a dynamic force spectroscopy experiment is conducted, the approach of the probe to the sample surface is carried out at a constant speed, i.e. the instantaneous changes of the cantilever deflection are continuously recorded. An example of the force curve obtained by dynamic force spectroscopy with a thermally driven cantilever in ambient conditions is shown in Figure 3.

Dynamic force spectroscopy experiment has been performed on HOPG in air (relative humidity is 55%, room temperature is 296 K, atmospheric pressure) with constant approach velocity of 0.82 nm/ms and rectangular Au-coated silicon cantilever with the cantilever first free flexural eigenmode at a frequency of 11.8 kHz and spring constant equals 0.14 N/m (measured using thermal tune method applied to the first flexural mode [13]). The inverse optical lever sensitivity [28] is equal to 186.32 nm/V.

In Figure 3, the free oscillations around the zero deflection line due to the thermal excitation of the tip approaching the surface correspond to the negative part of the time scale. A sharp downward deflection (of the order of 4 nm) near zero time corresponds to the jump-to-contact (JTC) transition. The contact line, which shows the cantilever behavior, when the tip is in contact with the sample surface after the JTC transition, corresponds to the positive part of the time scale.

Analysis of the force curve (Fig. 3) by the Fourier transform is presented in Figure 4. On the Fourier power spectrum (Fig. 4a) few resonance peaks (labeled 1, 2, 3, 4) can be seen. The highest peak at a frequency of 11.6 kHz clearly corresponds to the first flexural mode. The peak number 2 has frequency of 16.1 kHz and cannot be the second flexural mode of the cantilever. The frequency of the second flexural mode should be equal to 73.9 kHz, since it is 6.27 times higher than the first one [13];

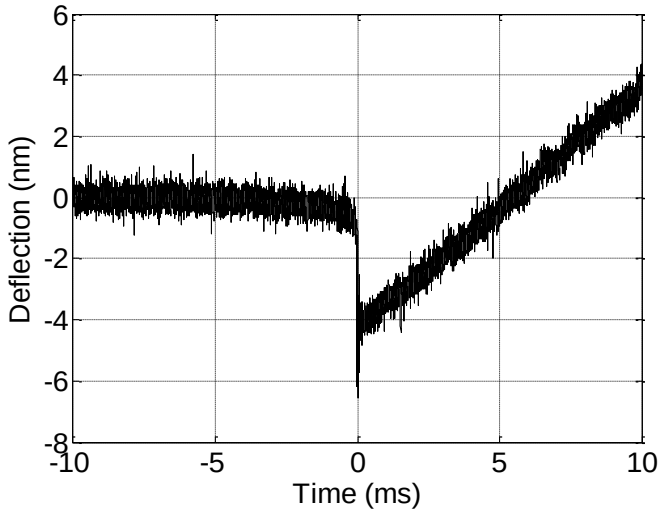

Figure 3. Deflections of the cantilever as a function of time during the dynamic force spectroscopy experiment measured by a standard optical beam deflection system.

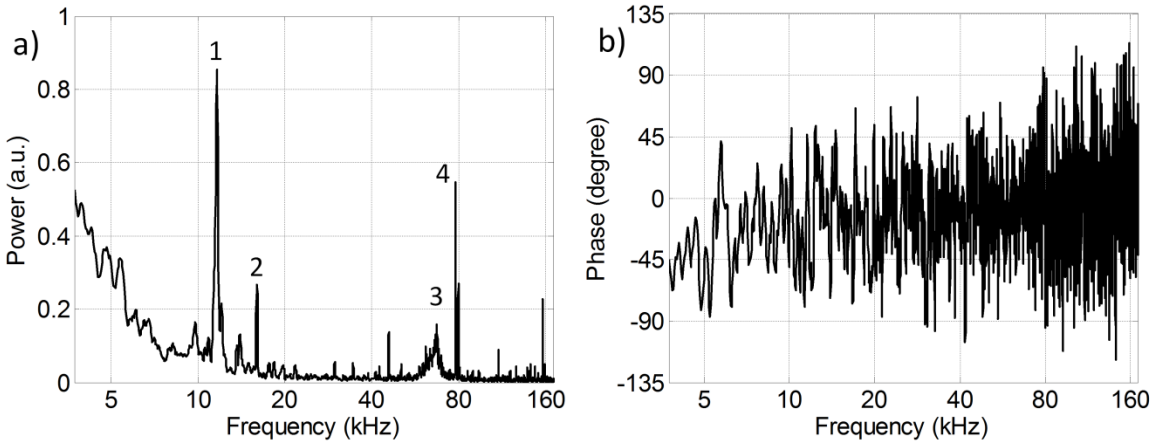

Figure 4. Fourier power (a) and phase (b) spectra of the signal shown in Figure 3. The frequency axes on both frames have base-2 logarithm scales.

hence, either peak number 3 at a frequency of 65.9 kHz, or number 4 at a frequency of 77.4 kHz, could be assigned to the second flexural mode. It is not possible to make an appropriate assignment just from the FT spectra. Moreover, it is worth noting that during the dynamic force spectroscopy experiment the cantilever eigenmodes structure is constantly changing due to the variation of external forces and boundary conditions, but Fourier spectrum in Figure 4a is the result of averaging over 20 ms, and it does not show the development of the spectrum in time. To attribute the FT spectral components of the signal, we look at the WT spectrum.

The analysis of the force curve (Fig. 3) by using the wavelet transform with the mother wavelet Morlet [20, 29] is presented in Figure 5. On the negative part of the time scale, the free oscillations of the first (bright yellow line) and the second (light blue line) flexural modes of the cantilever approaching the surface (Fig. 3) can be seen. The first flexural mode of the free cantilever on WT spectrum has a frequency of 11.9 kHz, that is down shifted before the JTC transition (here the tip approaches the surface and the tip-sample force gradient is responsible for this phenomenon). The second flexural mode has a frequency of 78.1 kHz. On the wavelet spectrum, it is easy to attribute the observed frequencies, in contrast to the Fourier spectrum.

The zero on the time scale corresponds to the JTC transition and is accompanied by several changes in the spectrum: spectral broadening around the first flexural mode and excitation in a short time interval of the second flexural mode at a frequency of 62.2 kHz. The detailed analysis of the signal around JTC transition is given in [23, 24].

On the positive part of the time scale, i.e. the oscillations of the cantilever after the JTC transition (Fig. 3), we note a resonance at a frequency of 16.3 kHz (light blue line at the bottom), slightly higher than the first free flexural mode, and a higher resonance at almost the same frequency as the second free flexural mode (light blue line at the top).These changes in spectrum are interesting because they cannot be attributed to the flexural modes of the pinned cantilever and, hence, suggest the existence of a complex interplay between the tip and the sample surface. The detailed analysis of this phenomenon on various surfaces can be found in [24].

Considering the WT spectra evolution (Fig. 5), the FT spectral components of the signal in Figure 4a can be easily attributed, since the temporal evolution of the peaks is shown as follows: peak number 2 corresponds to the frequency that appears after JTC and is a modified first free flexural mode, peak number 3 is caused by the excitation of the second flexural mode during the JTC, and peak number 3 is the second flexural mode of the cantilever.

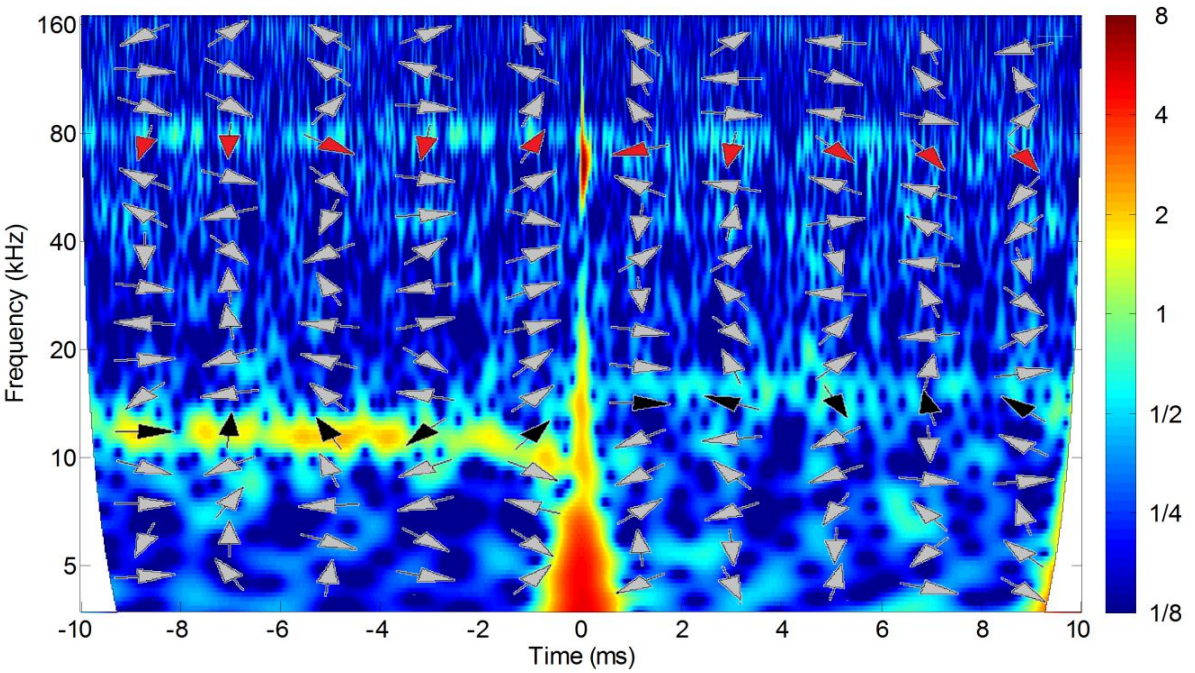

Figure 5. Wavelet transform of the signal shown in Figure 3. Wavelet coefficients are coded in color-scale. Both color-scale and frequency axes have base-2 logarithm scales. Edge artifacts of the WT are delimited by a white shade. The relative phase obtained as a result of the wavelet cross-correlations between the analyzed signal and the *sinc* function is coded in the slope of the arrows as in Figure 2. Black arrows correspond to the first flexural mode, red arrows belong to the second flexural mode, and gray arrows refer to all other frequencies.

The XWT phase measurements are coded in the slope of the arrows (Fig. 5). Black arrows correspond to the first flexural mode, red arrows belong to the second flexural mode, and gray arrows refer to all other frequencies. The measurements were carried out using the *sinc* function as a reference. In Figure 5, the XWT measurements before the JTC have been done with the time interval equals 25T (about 2 ms), where T is the oscillation period of the first flexural mode. In this case, the phase shift of the first flexural mode with respect to the translated *sinc* function should remain constant, if the cantilever oscillation is described by a pure sinusoid, as explained in section 2. However, it can be seen that the phase shift changes randomly over time. This is due to the fact that the observed signal is the response of the cantilever to the thermal excitation or thermal noise. The thermal excitation is a wideband random excitation constituted by molecular impacts on the cantilever by the molecules of the surrounding air in thermal agitation. As a consequence, the driving force acting on the cantilever is totally uncorrelated in time. From the XWT analysis, it appears that black and red arrows rotate randomly in time at the cantilever flexural modes, being a distinctive sign of the phase uncorrelation of the thermal excitation.

After JTC transition, cantilever is spring-coupled to the surface [24] and the resonance frequency of the first flexural mode as well as its oscillation period change (Fig. 5). XWT measurements after the JTC have been performed in the same way as for free oscillations. XWT measurements have been done with a time interval equals 30T' (~ 2 ms), where T' is the oscillation period of the first flexural mode after JTC. It can be seen that the relative phase shift of the first and second modes after JTC changes randomly within the analysis time frame (black and red arrows rotate). Again, XWT analysis provides an observation of the phase uncorrelation of the thermal excitation. Depth analysis is beyond the scope of the present work; however, this example shows possibility of XWT technique to access the phase of all spectral components of the signal simultaneously and at the time moments of interest, unlike FT, which gives phase spectra averaged over the entire acquisition time interval (Fig. 4b).

4. Conclusions

Wavelet analysis has been already successfully used to perform multi-frequency data analysis in AFM [22-25]; however, the whole range of its possibilities as a data analysis technique is not fully explored. With an appropriate theory, the WT can make a significant contribution to the definition of the samples surface properties that cannot be readily measured using other methods. This is ensured by the fact that the WT allows time-frequency analysis for each oscillating frequency of the cantilever, being able to extract such information without averaging. Using WT along with XWT analysis allows detecting the phases of the oscillating frequencies over time, thus providing additional valuable information on the signal.

The joint use of FT and WT provides the most comprehensive analysis of the signal [23-25], allowing to attribute the spectral components correctly, both in the wavelet spectrum and in the Fourier spectrum.

The approach discussed in this work is of great potential for the development of AFM, but it can be applied in various fields of science, where rapidly varying and non-stationary signals need to be investigated.

References

[1] Binnig G, Quate C C and Gerber C 1986 *Phys. Rev. Lett.* **56** 930
[2] Raman A, Melcher J and Tung R 2008 *Nano Today* **3** 20
[3] Garcia R and Herruzo E T 2012 *Nature Nanotech.* **7** 217
[4] Stark R W 2010 *Materials today* **13** 24
[5] Sahin O and Alatar A 2001 *Appl. Phys. Lett.* **79** 4455
[6] Balantekin M and Alatar A 2005 *Appl. Phys. Lett.* **87** 243513
[7] Hembacher S, Giessibl F J and Mannhart J 2004 *Science* **305** 380
[8] Sebastian A, Salapaka M V, Chen D J and Cleveland J P 1999 *Proc. American Control Conf. (San Diego)* vol 1 (San Diego: IEEE) pp 232-6
[9] Hu S, Howell S, Raman A, Reifenberger R and Franchek M 2004 *J. Vib. Acoust.* **126** 343
[10] Stark R W and Heckl W M 2003 *Rev. Sci. Instrum.* **74** 5111
[11] Schiener J, Witt S, Stark M and Guckenberger R 2004 *Rev. Sci. Instrum.* **75** 2564
[12] Raman A, Trigueros S, Cartagena A, Stevenson A P Z, Susilo M, Nauman E and Contera S A 2011 *Nature Nanotech.* **6** 809
[13] Butt H J and Jaschke M 1995 *Nanotechnology* **6** 1
[14] Lozano J R and Garcia R 2008 *Phys. Rev. Lett.* **100** 076102
[15] Martinez N F, Patil S, Lozano J R and Garcia R 2006 *Appl. Phys. Lett.* **89** 153115
[16] Stark R W and Heckl W M 2000 *Surf. Sci.* **457** 219
[17] Xu X and Raman A 2007 *J. Appl. Phys.* **102** 034303
[18] Giessibl F J 2003 *Rev. Mod. Phys.* **75** 949
[19] Garcia R and Perez R 2002 *Surf. Sci. Reports* **47** 197
[20] Mallat S 1999 *A Wavelet Tour of Signal Processing* (San Diego: Academic Press)
[21] Pukhova V, Gorelova E, Ferrini G and Burnasheva S 2017 *Proc. 2017 IEEE Russia Section Young Researchers in Electrical and Electronic Engineering Conf. (2017 ElConRus) (St.Petersburg)* (St.Petersburg: IEEE) 16839467
[22] Malegori G and Ferrini G 2010 *Beilstein J. Nanotechnol.* **1** 172
[23] Pukhova V, Banfi F and Ferrini G 2013 *Nanotechnology* **24** 505716
[24] Pukhova V, Banfi F and Ferrini G 2015 *Nanotechnology* **26** 175701
[25] Pukhova V, Banfi F and Ferrini G 2014 *Beilstein J. Nanotechnol.* **5** 494
[26] Butt H J, Cappella B and Kappl M 2005 *Surf. Sci. Reports* **59** 1
[27] Cappella B and Dietler G 1999 *Surf. Sci. Reports* **34** 1
[28] Higgins M J, Proksch R, Sader J E, Polcik M, Mc Endoo S, Cleveland J P and Jarvis S P 2006 *Rev. Sci. Instrum.* **77** 013701
[29] Deng Y, Wang C, Chai L and Zhang Z 2005 *Appl. Phys.* B **81** 1107